RSC Advances

PAPER

View Article Online
View Journal | View Issue

Cite this: *RSC Adv.*, 2020, **10**, 41324

Mechanical properties of $CrFeCoNiCu_x$ ($0 \leq x \leq 0.3$) HEAs from first-principles calculations

Yu Liu,[ab] Zhipeng Wang,[c] Hui Xiao,[d] Gang Chen,*[a] Touwen Fan*[b] and Li Ma[e]

Received 29th September 2020
Accepted 6th November 2020

DOI: 10.1039/d0ra08322d

rsc.li/rsc-advances

Frist-principles calculations combined with exact muffin-tin orbitals (EMTO) and coherent potential approximation (CPA) methods are conducted to investigate the effects of Cu content on mechanical properties of $CrFeCoNiCu_x$ ($0 \leq x \leq 0.3$) high-entropy alloys (HEAs), and the dependencies of relevant physical parameters on Cu content in HEAs are shown and discussed in this work. It is found that the equilibrium lattice constant increases linearly and the elastic constant decreases gradually with increasing Cu content, and the crystal structure of $CrFeCoNiCu_x$ ($0 \leq x \leq 0.3$) HEAs can preserve mechanical stability according to the stability criterion of cubic crystals. From the general trend, adding Cu atoms to CrFeCoNi-based HEAs will reduce elastic moduli, Vickers hardness, and yield strength, whereas ductility and plasticity of HEAs show the opposite trend. Also, three different dislocations, including screw, edge, and mixed dislocations, and twins are more likely to occur in HEAs with high Cu content because energy factors decrease steadily and dislocation widths increase gradually with increasing Cu content. The present results provide valuable theoretical verification for further research on the mechanical properties of $CrFeCoNiCu_x$ ($0 \leq x \leq 0.3$) HEAs.

1 Introduction

An alloy with five or more principal elements in equiatomic or nearly equiatomic proportions is called a high entropy alloy (HEA), which was first introduced by Yeh *et al.* and Cantor *et al.* in 2004.[1,2] Due to the high entropy,[3] severe lattice distortion,[4] sluggish diffusion,[5] and Cocktail effects,[6] promoting the alloy forms a simple solid solution, such as a face-centered cubic (fcc) phase, body-centered cubic (bcc) phase or hexagonal close-packed (hcp) phase or their mixtures, rather than a complex crystal structure with multiple phases and intermetallic compounds.[7–12] Moreover, making the special mixture reflects many outstanding properties, including high hardness,[8] high strength,[13] corrosion resistance,[14] wear resistance,[15] and electromagnetic properties,[16] which cannot be matched by traditional alloys. Thereby, HEAs have become one of the hotspots in material research in recent years. In addition, first-principles calculations has been widely applied and proved to be effective in studying the physical properties of different materials, *e.g.*, mechanical properties,[17] hydrogen embrittlement,[18,19] antioxidation mechanism,[20,21] and thermodynamic properties,[22] thus theoretical analysis is a significant means to reveal the intrinsic properties of materials.

To date, the properties of HEA systems composed of Fe, Co, Cr, Ni, Mn, Al, Cu, Mo, and Ti elements have become the research focus and a lot of related studies have been done. For experimental researches, Shun *et al.*[23] produced four modified $CoCrFeNiAl_{0.3}$, $CoCrFeNiTi_{0.3}$, $CoCrFeNiMo_{0.3}$, and $CoCrFeNiAl_{0.3}Mo_{0.1}$ HEAs, and investigated their microstructures to understand the relationships between nanoparticle formation/ordering and alloy composition for fcc HEAs, the results revealed that the formation of nanoparticles was mainly affected by the high mixing entropy, sluggish cooperative diffusion of atoms, and negative mixing enthalpies. Fu *et al.*[24] observed the formation of 5 vol% nano-twins in the bulk $Co_{25}Ni_{25}Fe_{25}Al_{7.5}Cu_{17.5}$ HEA, and found that the alloy exhibited a hardness of 454 HV and a compressive yield strength of 1795 MPa, which was much higher than that of most previously reported HEAs with fcc crystal structure (130–700 MPa). Zhao *et al.*[25] studied the effects of Cr content on phase formation and magnetic properties of $CoCr_xCuFeMnNi$ ($x = 0$, 0.5, 1.0, 1.5, 2.0 mol) HEAs, and the results showed that the alloys milled for 50 h formed a single fcc phase when Cr content was below 1.5 mol, whereas the phase structure consisted of fcc and bcc phases when Cr content was between 1.5 and 2.0 mol, and the soft magnetic properties decreased gradually with the increase in Cr content, which was attributed to the decrease in the content of ferromagnetic components and the formation of bcc

[a]College of Materials Science and Engineering, Hunan University, Changsha, Hunan, 410082, P. R. China. E-mail: chengang@hnu.edu.cn
[b]Research Institute of Automobile Parts Technology, Hunan Institute of Technology, Hengyang, Hunan, 421002, P. R. China. E-mail: fantouwen_1980@163.com
[c]School of Material Science and Energy Engineering, Foshan University, Foshan, Guangdong, 528001, P. R. China
[d]School of Mechatronics Engineering, Foshan University, Foshan, Guangdong, 528001, P. R. China
[e]Key Laboratory of New Electric Functional Materials of Guangxi Colleges and Universities, Nanning Normal University, Nanning, Guangxi, 530023, P. R. China

phase. Gludovatz *et al.*[7] studied the mechanical properties of equiatomic CrMnFeCoNi HEA at a cryogenic temperature of 77 K, and found that the alloy had excellent fracture toughness above 200 MPa $m^{1/2}$ and tensile strength exceeding 1000 MPa. For theoretical studies, Ma *et al.*[26] applied the finite-temperature *ab initio* methods to investigate the thermodynamic properties of CoCrFeMnNi HEA, indicated that the variation of vibrational entropy, electronic entropy, configuration entropy, and magnetic entropy among the various phases induces a strong spread in the corresponding entropy contributions and thus affects phase stability differences markedly. Meanwhile, on the basis of exact muffin-tin orbitals (EMTO) and coherent-potential approximation (CPA),[27] Sun *et al.*[28] studied the phase selection rule of paramagnetic Al_x-CrMnFeCoNi ($0 \leq x \leq 5$) HEAs with fcc and bcc phases, and the results showed that the crystal structure of the alloys transformed from fcc phase to bcc phase with increasing Al content in the range of $0.482 < x < 1.361$. Huang[29] explored the ordering-induced elastic anomaly in the $FeCoNiAl_{1-x}Ti_x$ ($0 \leq x \leq 1$) HEAs by first-principles calculations, and the existence of $L1_2$ phase was the reason for the strong stability of shear deformation of Ti rich components. In addition, Singh *et al.*[30] proved the existence of short-ranged order (SRO) structure in AlCoCrFeNi HEA by the thermodynamic theory of electronic structure.

According to above researches, the experimental and theoretical studies on the physical properties of HEAs have been extensively carried out. However, the theoretical analysis on the mechanical properties of HEA systems consisted of Fe, Co, Cr, Ni, Mn, Al, Cu, Mo, and Ti elements is still insufficient. Therefore, this paper aims to study one of the HEA systems, $CrFeCoNiCu_x$ ($0 \leq x \leq 0.3$) HEAs with fcc crystal structure, and analyze the effects of Cu content on mechanical properties of the HEAs by first-principles calculations combined with the EMTO-CPA method. Physical parameters, such as elastic constants, elastic moduli, Poisson's ratios, Pugh's ratio, and so on, are calculated for the HEAs with different Cu contents, and the corresponding variation curves are displayed and discussed. The present results provide a valuable theoretical guidance for studying high-performance $CrFeCoNiCu_x$ ($0 \leq x \leq 0.3$) HEAs in the future.

2 Computational details

In this work, the EMTO-CPA method based on the density functional theory (DFT) was used to investigate the effects of Cu content on mechanical properties of $CrFeCoNiCu_x$ ($0 \leq x \leq 0.3$) HEAs with fcc crystal structure. The EMTO method was an effective theoretical approach for solving the Kohn–Sham equations to obtain the exact single-electron potential under the optimized overlapping muffin-tin potential spheres and calculating the total energy by the full charge-density technique.[28,31–33] The CPA was a single-site mean-field approximation theory to deal with the substitutional disorder of chemical and magnetic degrees of freedom, herein, the local lattice relaxation effects and atomic short-range order were ignored completely.[34–36] The generalized gradient approximation (GGA) of Perdew–Burke–Ernzerhof (PBE) was selected as the exchange–correlation functional to obtain the charge density and total energy.[28] The electronic states of s, p, d, and f orbitals of EMTO basis set was optimized.[37] Moreover, a rigorous *k*-points convergence test is conducted by Brillouin zone integrations before calculation, and then the *k*-points of $29 \times 29 \times 29$ are chosen to ensure the accuracy of all energies and energy differences between different crystal lattices.[38] The Green's function of 16 complex energy points distributed on the Fermi surface was solved.[32] The calculated energy-volume data were accurately fitted by the Morse-type function[39] to obtain the equilibrium volume, and the thermal contribution was ignored because all calculations were based on static lattice.

3 Results and discussions

According to the set conditions, the equilibrium lattice constant a_0 of $CrFeCoNiCu_x$ ($0 \leq x \leq 0.3$) HEAs is calculated firstly, and then the corresponding variation curve of the physical parameter *versus* Cu content for the HEAs is displayed in Fig. 1. Clearly, it can be seen that the value of equilibrium lattice constant a_0 gradually increases in a linear form with the increase in Cu content from 0 to 0.3, which shows that Cu atom addition to CrFeCoNi-based HEAs will reduce the interaction between atoms, thereby causing the lattice expansion. Meanwhile, we compare the calculated lattice constants with available experimental and theoretical data for CrFeCoNi and CrFeCoNiCu HEAs, as listed in Table 1. It can be found that the corresponding theoretical predications are 3.578 Å and 3.590 Å, respectively, which are very close to the previous experimental data for CrFeCoNi and CrFeCoNiCu HEAs,[40–44] and the theoretical data for CrFeCoNi HEA,[42,45] the comparison results verify the validity of the theoretical analysis method.

Meanwhile, we calculate the elastic constants C_{11}, C_{12}, and C_{44} of $CrFeCoNiCu_x$ ($0 \leq x \leq 0.3$) HEAs due to their cubic crystal structure, and the variation curves of elastic constants C_{ij} *versus* Cu content are illustrated in Fig. 2. On the basis of the calculated results, it can be found that the overall variation trend of these three parameters is gradually decreasing with the increase

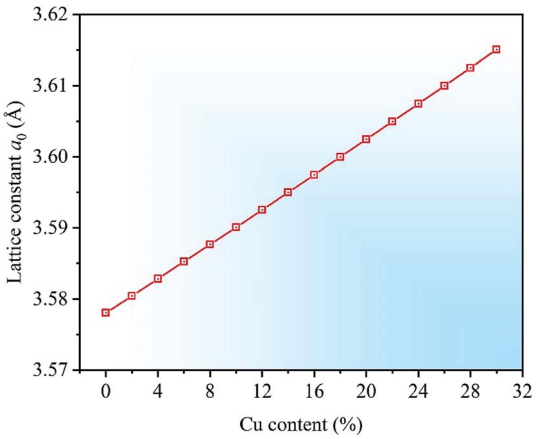

Fig. 1 Calculated lattice constant a_0 as a function of Cu content for $CrFeCoNiCu_x$ ($0 \leq x \leq 0.3$) HEAs.

Table 1 Comparisons of calculated lattice constants with previous experimental and theoretical data for CrFeCoNi and CrFeCoNiCu HEAs

a_0 (Å)	Present	Experimental data	Theoretical data
CrFeCoNi	3.578	3.572,[40] 3.574,[41] 3.575 (ref. 42)	3.540,[42] 3.568 (ref. 45)
CrFeCoNiCu	3.590	3.579,[40] 3.584,[43] 3.595 (ref. 44)	—

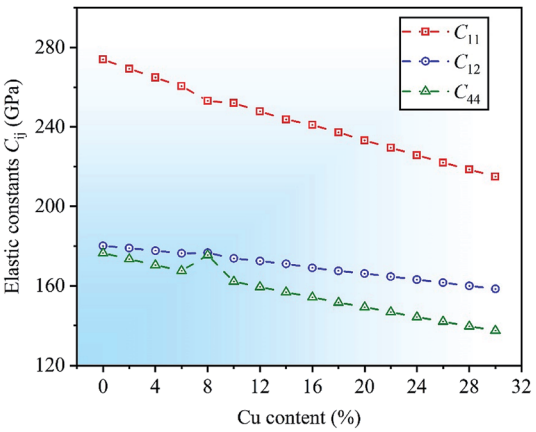

Fig. 2 Calculated elastic constants C_{ij} as a function of Cu content for CrFeCoNiCu$_x$ ($0 \le x \le 0.3$) HEAs.

in Cu content, although there is an obvious fluctuation for the elastic constant C_{44} when Cu content is in the range of 6–10%, suggesting that the capability to resist external forces declines with increasing Cu content. And the remarkable enhancement of elastic constant C_{44} shows that the deformation resistance of materials increases at 6–10% Cu concentration, which may be induced by the structural phase transition due to severe lattice distortion in HEAs, but the specific reasons cannot be obtained by using the EMTO-CPA method yet. In addition, the calculated elastic constants C_{ij} must meet the stability criterion of cubic crystals,[46] the corresponding relationships are formulized by the following eqn (1). Hence, according to the calculated results in Fig. 2, it can be seen that the elastic constants C_{ij} always satisfy the constraint conditions at different Cu contents, which indicates that the cubic crystal structure of CrFeCoNiCu$_x$ ($0 \le x \le 0.3$) HEAs can maintain mechanical stability. To verify the validity of the calculated results, we compare the theoretical predictions with available research results for CrFeCoNi HEA, the present values are respectively C_{11} = 273.9 GPa, C_{12} = 180.1 GPa, and C_{44} = 176.5 GPa, which agree well with the previous research data C_{11} = 271.0 GPa, C_{12} = 175.0 GPa, and C_{44} = 189.0 GPa.[32]

$$C_{11} > 0,\ C_{44} > 0,\ (C_{11} - C_{12}) > 0,\ (C_{11} + 2C_{12}) > 0 \quad (1)$$

To study the mechanical properties of CrFeCoNiCu$_x$ ($0 \le x \le 0.3$) HEAs, we first calculate three important elastic moduli, such as bulk modulus B, shear modulus G, and Young's modulus E, to evaluate the deformation resistance of materials. According to reference,[47] the elastic moduli are related to the elastic constants C_{ij}, the calculation expressions are formulized by the following eqn (2)–(4), in which G_V and G_R are respectively the Voigt and Reuss shear moduli.[48] The theoretical predictions are presented in Fig. 3a, it can be seen that the elastic moduli of CrFeCoNiCu$_x$ ($0 \le x \le 0.3$) HEAs decrease gradually with increasing Cu content, indicating that Cu atom addition to CrFeCoNi-based HEAs will reduce the deformation resistance of materials, and it has the greatest influence on the elastic deformation resistance of alloys. Meanwhile, the results show that CrFeCoNi HEA has the best deformation resistance with respect to other CrFeCoNiCu$_x$ ($0 < x \le 0.3$) HEAs. According to the calculated data, the three elastic moduli of CrFeCoNi HEA are respectively B = 211.4 GPa, G = 104.2 GPa, and E = 268.5 GPa, which fit well with the previous research results B = 207.0 GPa, G = 110.0 GPa, and E = 280.0 GPa,[49] the comparison results show that the calculated data are accurate.

$$B = (C_{11} + 2C_{12})/3 \quad (2)$$

$$G = (G_V + G_R)/2 \quad (3)$$

$$E = 9BG/(3B + G) \quad (4)$$

In addition, we calculate other elastic moduli, $G_{(100)[010]}$, $G_{(110)[1\bar{1}0]}$, and $E_{[100]}$, to further study the deformation resistance of CrFeCoNiCu$_x$ ($0 \le x \le 0.3$) HEAs. Herein, $G_{(100)[010]} = C_{44}$ and $G_{(110)[1\bar{1}0]} = (C_{11} - C_{12})/2$ represent respectively the resistance to shear deformation of crystal structure in the (100)[010] and (110)[1$\bar{1}$0] directions, and $E_{[100]} = (C_{11} - C_{12})(1 - C_{12})/(C_{11} + C_{12})$ is the resistance to elastic deformation in the [100] crystallographic direction.[50,51] Through calculation, we display the calculated results of these three elastic moduli in Fig. 3b. Obviously, the values of elastic moduli $G_{(100)[010]}$, $G_{(110)[1\bar{1}0]}$, and $E_{[100]}$ have the similar trend that the overall trend of each parameter is gradually decreasing, although each variation curve has an obvious fluctuation at 6–10% of Cu content, suggesting that the deformation resistance of CrFeCoNiCu$_x$ ($0 \le x \le 0.3$) HEAs in the three different crystallographic directions also decreases with increasing Cu content, and CrFeCoNi HEA has the best deformation resistance in nature.

Pugh's ratio B/G is a significant physical parameter, which is usually used to determine the ductility or brittleness of materials, and the critical value of ductile–brittle transition is 1.75.[52,53] Herein, we calculate the ratio of CrFeCoNiCu$_x$ ($0 \le x \le 0.3$) HEAs according to the calculated elastic moduli B and G, and the corresponding variation curve is displayed in Fig. 4. Clearly, the calculated results are always greater than 1.75 in the range of 0–30%, which indicates that CrFeCoNiCu$_x$ ($0 \le x \le 0.3$)

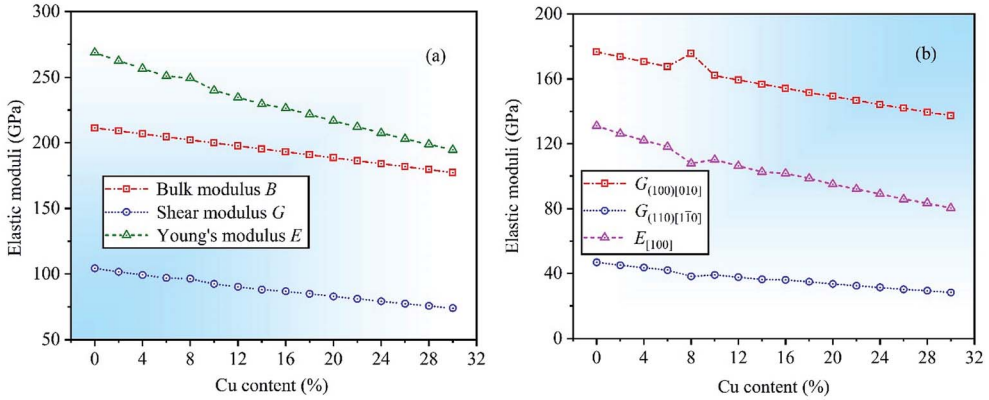

Fig. 3 Calculated (a) and (b) elastic moduli as a function of Cu content for $CrFeCoNiCu_x$ ($0 \le x \le 0.3$) HEAs.

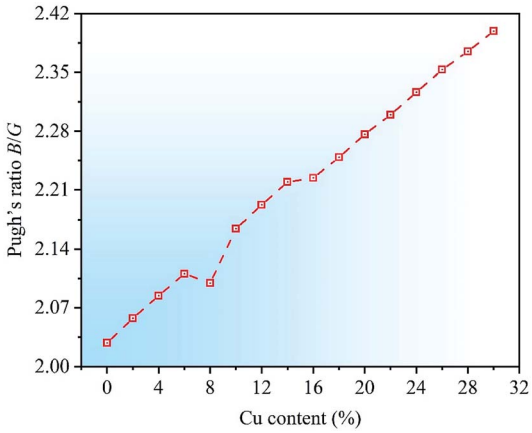

Fig. 4 Calculated Pugh's ratio B/G as a function of Cu content for $CrFeCoNiCu_x$ ($0 \le x \le 0.3$) HEAs.

HEAs are ductile materials, and Cu atom addition to CrFeCoNi-based HEAs can increase the ductility of alloys as a whole, thereby $CrFeCoNiCu_{0.3}$ HEA has the best ductility compared with other HEAs with different Cu contents. The curve has a marked downward fluctuation when Cu content is in the range of 6% and 10%, indicating that the ductility of $CrFeCoNiCu_x$ ($0.06 \le x \le 0.1$) HEAs decreases dramatically, and the interesting phenomenon may be related to the severe lattice distortion of HEAs.

Plasticity is one of the significant physical properties of materials to evaluate the capability to resist plastic deformation. In this work, we calculate respectively Poisson's ratios $\sigma_{[001]}$ and $\sigma_{[111]}$ to determine the plastic property of $CrFeCoNiCu_x$ ($0 \le x \le 0.3$) HEAs in the [001] and [111] crystallographic directions, the calculation expressions are formulized by the following eqn (5) and (6),[54] and the calculated results are depicted in Fig. 5. According to the calculated results, the overall trend of $\sigma_{[001]}$ and $\sigma_{[111]}$ is slowly increasing with the increase in Cu content, reflecting that adding Cu atom to CrFeCoNi-based HEAs can increase the plastic property of materials in the [001] and [111] crystallographic directions. However, when Cu content is in the range of 6% and 10%, the calculated values of $\sigma_{[001]}$ and $\sigma_{[111]}$ show different trends, which indicates that the corresponding Cu content has opposite effect on the plastic property of $CrFeCoNiCu_x$ ($6 \le x \le 10$) HEAs in the [001] and [111] directions. Moreover, Poisson's ratio $\sigma_{[111]}$ gets the minimum value when Cu content is 8%, indicating that $CrFeCoNiCu_{0.08}$ HEA has the worst plasticity compared to other HEAs with different Cu contents in the [111] crystallographic direction. Additionally, $CrFeCoNiCu_{0.3}$ HEA is the best plastic material in the two crystallographic directions according to the variation curves.

$$\sigma_{[001]} = \frac{C_{12}}{C_{11} + C_{12}} \tag{5}$$

$$\sigma_{[111]} = \frac{C_{11} + 2C_{12} - 2C_{44}}{2(C_{11} + 2C_{12} + C_{44})} \tag{6}$$

In addition, Vickers hardness H_v and yield strength σ_y are calculated to further investigate the mechanical properties of $CrFeCoNiCu_x$ ($0 \le x \le 0.3$) HEAs. According to reference,[55,56] the formulas are respectively $H_v = 2(k^2G)^{0.585} - 3$ and $\sigma_y = H_v/3$, where $k = G/B$. Through calculation, the theoretical predictions are depicted in Fig. 6. We can find that the total trend of

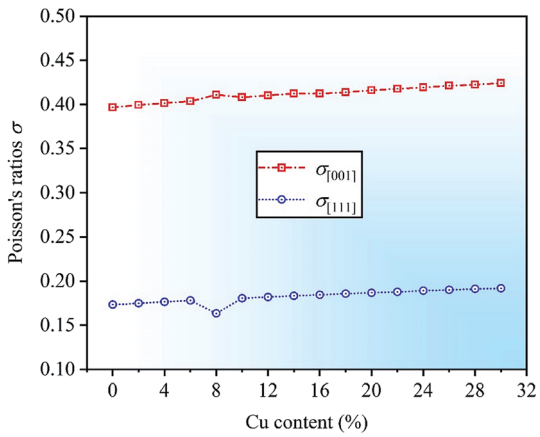

Fig. 5 Calculated Poisson's ratios σ as a function of Cu content for $CrFeCoNiCu_x$ ($0 \le x \le 0.3$) HEAs.

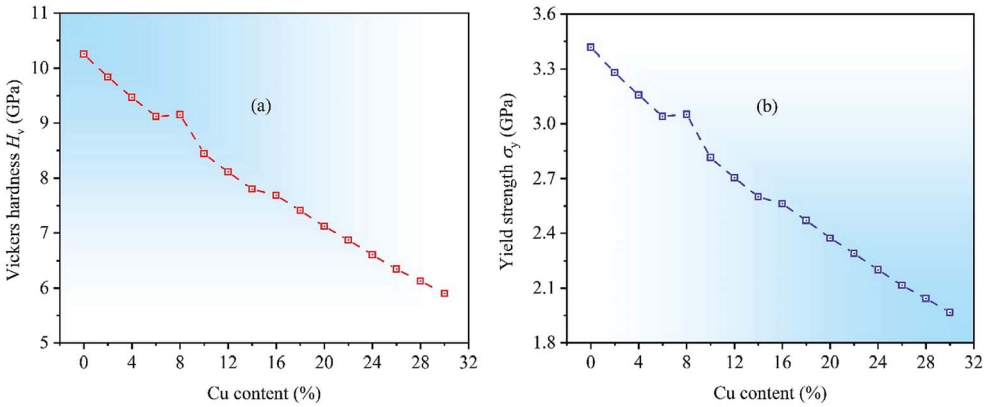

Fig. 6 Calculated (a) Vickers hardness H_v and (b) yield strength σ_y as a function of Cu content for $CrFeCoNiCu_x$ ($0 \le x \le 0.3$) HEAs.

variation curves is gradually decreasing with increasing Cu content in the range of 0–30%, though the values of two physical parameters have upward fluctuations when Cu contents are in the range of 6% and 10%, and the results indicate that Cu addition to CrFeCoNi-based HEAs will decrease the Vickers hardness and yield strength of materials as a whole, namely, the Vickers hardness and yield strength of CrFeCoNi HEA are better than those of other HEAs with different Cu contents in nature.

Elastic anisotropy is one of the significant characteristics for the crystal structure of HEAs due to the severe lattice distortion. Herein, we calculate anisotropy factors A_Z and $A_{(110)[001]}$ to study the effects of elastic anisotropy on mechanical properties of $CrFeCoNiCu_x$ ($0 \le x \le 0.3$) HEAs, and the calculated expressions are formulized by the following eqn (7) and (8),[54,57] where A_Z denotes the Zener ratio that the ratio of shear moduli between the (100) and (110) crystal planes,[58,59] $A_{(110)[001]}$ is the anisotropy factor of crystal structure in the (110)[001] direction, and $C' = C_{44} + (C_{11} + C_{12})/2$. Through calculation, the theoretical predictions of A_Z and $A_{(110)[001]}$ are displayed in Fig. 7. It can be seen that the general trend of variation curves is gradually rising with increasing Cu content, the result suggests that increasing Cu atom in CrFeCoNi-based HEAs will rise the elastic anisotropy of crystal structure, and it has the greatest effect on the anisotropy factor A_Z of materials. In addition, the values of A_Z and $A_{(110)[001]}$ increase dramatically when Cu content is 8%, suggesting that the lattice distortion in $CrFeCoNiCu_{0.08}$ HEA is severer than that in $CrFeCoNiCu_{0.06}$ and $CrFeCoNiCu_{0.1}$ HEAs. Meanwhile, it can be found that the large anisotropy factors correspond to the good plasticity and the worse deformation resistance of $CrFeCoNiCu_x$ ($0 \le x \le 0.3$) HEAs in conjunction with the previous calculations, the result is consistent with an important conclusion that the large elastic anisotropy is more likely to boost the cross slip of screw dislocations in crystalline materials.[60]

$$A_Z = \frac{2C_{44}}{C_{11} - C_{12}} \tag{7}$$

$$A_{(110)[001]} = \frac{C_{44}(C' + 2C_{12} + C_{11})}{C_{11}C' - C_{12}^2} \tag{8}$$

It is generally known that the capability of dislocation nucleation is closely related to the mechanical properties of crystalline materials, which can be quantified by means of energy factor K and the small value of K means that dislocations are more likely to nucleate in materials. In this work, we calculate respectively energy factors K_{screw} and K_{edge} to investigate the nucleation ability of screw and edge dislocations in $CrFeCoNiCu_x$ ($0 \le x \le 0.3$) HEAs, the corresponding formulas are written by the following eqn (9) and (10),[61,62] and the calculated results are displayed in Fig. 8. According to the calculated results, we can find that the values of K_{screw} and K_{edge} gradually decrease with increasing Cu content, which implies that the Cu addition to CrFeCoNi-based HEAs will increase the capability of dislocation nucleation in HEAs, and the high Cu content corresponds to the strong nucleation ability, therefore, the screw and edge dislocations are more likely nucleated in $CrFeCoNiCu_{0.3}$ HEA compared to the HEAs with other Cu contents. And the energy factor K_{screw} is always less than the energy factor K_{edge} in the set range of Cu content, indicating that the screw dislocation is more likely to nucleate in

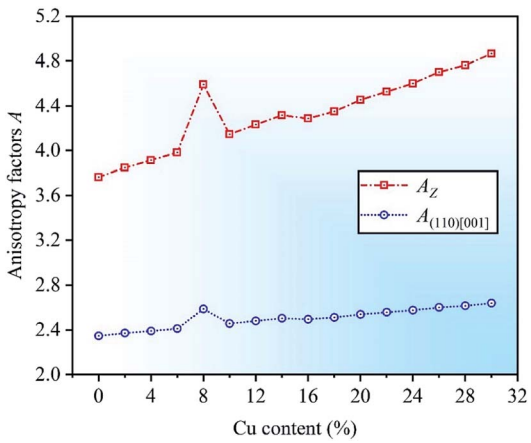

Fig. 7 Calculated anisotropy factors A as a function of Cu content for $CrFeCoNiCu_x$ ($0 \le x \le 0.3$) HEAs.

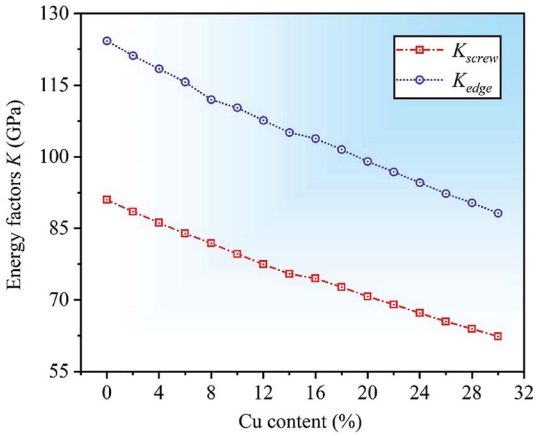

Fig. 8 Calculated energy factors K as a function of Cu content for $CrFeCoNiCu_x$ ($0 \le x \le 0.3$) HEAs.

$CrFeCoNiCu_x$ ($0 \le x \le 0.3$) HEAs compared to the edge dislocation.

$$K_{screw} = \sqrt{\frac{C_{44}(C_{11} - C_{12})}{2}} \quad (9)$$

$$K_{edge} = (C_{11} + C_{12})\sqrt{\frac{C_{44}(C_{11} - C_{12})}{C_{11}(C_{11} + C_{12} + 2C_{44})}} \quad (10)$$

And finally, we calculate the energy factor K_{mixed} and dislocation width ζ of mixed dislocation of $CrFeCoNiCu_x$ ($x = 0$, 0.1, 0.2, 0.3) HEAs to further study the dislocation properties of $CrFeCoNiCu_x$ ($0 \le x \le 0.3$) HEAs, and the calculated results are depicted in Fig. 9. The specified formulas are written by the following eqn (11) and (12),[61,63] in which θ ($0 \le \theta \le \pi$) denotes the direction angle between Burgers vector and dislocation line, $\theta = 0$ and $\theta = \pi/2$ correspond to the screw and edge dislocations, respectively, and d is the distance between glide planes. In Fig. 9a, we can find that the energy factor K_{mixed} of mixed dislocation gradually decreases with increasing Cu content, which indicates that the high Cu content is easier to promote the nucleation of mixed dislocation in $CrFeCoNiCu_x$ ($0 \le x \le 0.3$) HEAs. However, the varying trend of dislocation width ζ is opposite to that of energy factor K_{mixed} that the theoretical prediction of ζ gradually increases with increasing Cu content, as depicted in Fig. 9b, suggesting that Cu addition to CrFeCoNi-based HEAs is conducive to decrease the stacking-fault energy of the HEAs, thereby boosting the twinning deformation and improving the plasticity of HEAs.

$$K_{mixed} = K_{edge}\sin^2\theta + K_{screw}\cos^2\theta \quad (11)$$

$$\zeta = \frac{K_{mixed}d}{C_{11} - C_{12}} \quad (12)$$

4 Conclusions

In summary, the effects of Cu content on mechanical properties of $CrFeCoNiCu_x$ ($0 \le x \le 0.3$) HEAs are investigated in this work. It is demonstrated that Cu addition to CrFeCoNi-based HEAs will increase the equilibrium lattice constant and decrease the elastic constants as a whole, and the calculated lattice constant, elastic constants, and elastic moduli fit well with previous research results for CrFeCoNi HEA. The general varying trend of elastic moduli, Vickers hardness, and yield strength is gradually decreasing with increasing Cu content, though the corresponding variation curves have an obvious fluctuation when Cu content is in the range of 6% and 10%, indicating that HEAs with low Cu content may have better deformation resistance, whereas the ductility and plasticity of $CrFeCoNiCu_x$ ($0 \le x \le 0.3$) HEAs are reversed. When Cu content is 8%, $CrFeCoNiCu_{0.08}$ HEA has the worst plasticity in the [111] crystallographic direction because the Poisson's ratio $\sigma_{[111]}$ gets the minimum value, and $CrFeCoNiCu_{0.08}$ HEA has more severe lattice distortion compared to $CrFeCoNiCu_{0.06}$ and $CrFeCoNiCu_{0.1}$ HEAs due to the remarkable increase of anisotropy factors. The screw, edge, and mixed dislocations are more likely to nucleate in CrFeCoNi-based HEAs with high Cu content, and the screw dislocation is easily inclined to occur in $CrFeCoNiCu_x$ ($0 \le x \le 0.3$) HEAs compared to the edge dislocation. Adding Cu atoms to CrFeCoNi-based HEAs is beneficial to decrease the stacking-fault energy in HEAs, thereby boosting

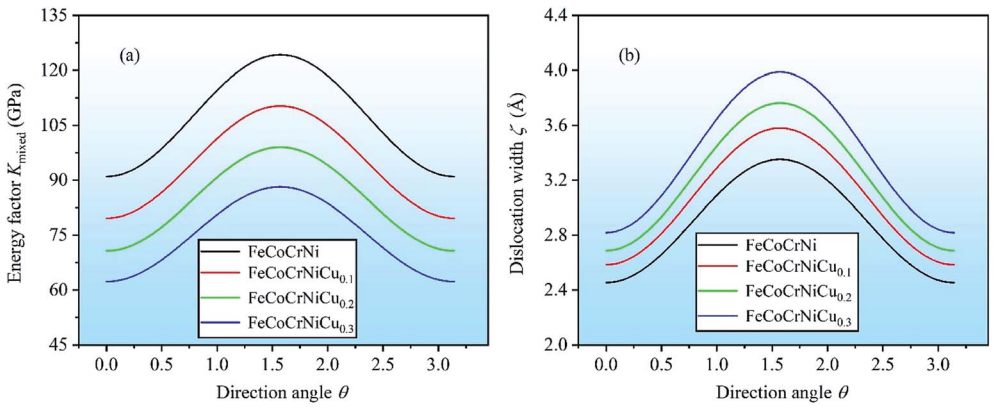

Fig. 9 Variation curves of (a) energy factor K_{mixed} and (b) dislocation width ζ *versus* direction angle θ($0 \le \theta \le \pi$) between Burgers vector and dislocation line.

the twinning deformation and improving the plasticity of HEAs. The present results provide a theoretical verification for studying the effects of Cu content on mechanical properties of $CrFeCoNiCu_x$ ($0 \leq x \leq 0.3$) HEAs, which is helpful for the optimal design and application of high-performance $CrFeCoNiCu_x$ ($0 \leq x \leq 0.3$) HEAs in the future.

Conflicts of interest

There are no conflicts to declare.

Acknowledgements

The authors greatly appreciate the support of National Natural Science Foundation of China (51971091), Guangdong Basic and Applied Basic Research Foundation (No. 2019A1515110274), Natural Science Foundation of Guangxi Province (No. 2017GXNSFAA198154), China Postdoctoral Science Foundation (No. 2018M642973), and Foshan University Scientific Research Project (No. CGG07257, CGG07026, BGH206017, and BGH206025). The authors deeply appreciate Prof. Levente Vitos for providing his developed codes of EMTO-CPA method for this work. This work is implemented in National Supercomputer Centers in Changsha, China.

References

1 J. W. Yeh, S. K. Chen, S. J. Lin, J. Y. Gan, T. S. Chin, T. T. Shun, C. H. Tsau and S. Y. Chang, *Adv. Eng. Mater.*, 2004, **6**, 299–303.
2 B. Cantor, I. T. H. Chang, P. Knight and A. J. B. Vincent, *Mater. Sci. Eng., A*, 2004, **375–377**, 213–218.
3 J. W. Yeh, *JOM*, 2013, **65**, 1759–1771.
4 C. Lee, G. Song, M. C. Gao, R. Feng, P. Y. Chen, J. Brechtl, Y. Chen, K. An, W. Guo, J. D. Poplawsky, S. Li, A. T. Samaei, W. Chen, A. Hu, H. Choo and P. K. Liaw, *Acta Mater.*, 2018, **160**, 158–172.
5 B. E. Macdonald, Z. Fu, B. Zheng, W. Chen, Y. Lin, F. Chen, L. Zhang, J. Ivanisenko, Y. Zhou, H. Hahn and E. J. Lavernia, *JOM*, 2017, **69**, 2024–2031.
6 S. Ranganathan, *Curr. Sci.*, 2003, **85**, 1404–1406.
7 B. Gludovatz, A. Hohenwarter, D. Catoor, E. H. Chang, E. P. George and R. O. Ritchie, *Science*, 2014, **345**, 1153–1158.
8 Z. D. Han, N. Chen, S. F. Zhao, L. W. Fan, G. N. Yang, Y. Shao and K. F. Yao, *Intermetallics*, 2017, **84**, 153–157.
9 M. Feuerbacher, M. Heidelmann and C. Thomas, *Mater. Res. Lett.*, 2015, **3**, 1–6.
10 W. R. Wang, W. L. Wang, S. C. Wang, Y. C. Tsai, C. H. Lai and J. W. Yeh, *Intermetallics*, 2012, **26**, 44–51.
11 Z. Li, K. G. Pradeep, Y. Deng, D. Raabe and C. C. Tasan, *Nature*, 2016, **534**, 227–230.
12 T. G. Novak, H. D. Vora, R. S. Mishra, M. L. Young and N. B. Dahotre, *Metall. Mater. Trans. B*, 2014, **45**, 1603–1607.
13 Y. H. Jo, K. Y. Doh, D. G. Kim, K. Lee, D. W. Kim, H. Sung, S. S. Sohn, D. Lee, H. S. Kim, B. J. Lee and S. Lee, *J. Alloys Compd.*, 2019, **809**, 151864.
14 Y. L. Chou, J. W. Yeh and H. C. Shih, *Corros. Sci.*, 2010, **52**, 2571–2581.
15 M. H. Chuang, M. H. Tsai, W. R. Wang, S. J. Lin and J. W. Yeh, *Acta Mater.*, 2011, **59**, 6308–6317.
16 S. Huang, A. Vida, A. Heczel, E. Holmstrom and L. Vitos, *JOM*, 2017, **69**, 2107–2112.
17 Y. Liu, K. Wang, H. Xiao, G. Chen, Z. P. Wang, T. Hu, T. W. Fan and L. Ma, *RSC Adv.*, 2020, **10**, 14080–14088.
18 Y. Pan and W. M. Guan, *Int. J. Hydrogen Energy*, 2020, **45**, 20032–20041.
19 Y. Pan, *Int. J. Hydrogen Energy*, 2019, **44**, 18153–18158.
20 Y. Pan, D. L. Pu and Y. L. Jia, *Vacuum*, 2020, **172**, 109067.
21 Y. Pan, D. L. Pu, Y. Q. Li and Q. H. Zheng, *Mater. Sci. Eng., B*, 2019, **259**, 114580.
22 Y. Pan, Y. H. Lin, G. H. Liu and J. Zhang, *Vacuum*, 2020, **174**, 109203.
23 T. T. Shun, C. H. Hung and C. F. Lee, *J. Alloys Compd.*, 2010, **493**, 105–109.
24 Z. Q. Fu, W. P. Chen, H. M. Wen, D. L. Zhang, Z. Chen, B. L. Zheng, Y. Z. Zhou and E. J. Lavernia, *Acta Mater.*, 2016, **107**, 59–71.
25 R. F. Zhao, B. Ren, G. P. Zhang, Z. X. Liu, B. Cai and J. J. Zhang, *J. Magn. Magn. Mater.*, 2019, **491**, 165574.
26 D. Ma, B. Grabowski, F. Körmann, J. Neugebauer and D. Raabe, *Acta Mater.*, 2015, **100**, 90–97.
27 L. Vitos, *Computational quantum mechanics for materials engineers: the EMTO method and applications*, Springer, London, 2007.
28 X. Sun, H. L. Zhang, S. Lu, X. D. Ding, Y. Z. Wang and L. Vitos, *Acta Mater.*, 2017, **140**, 366–374.
29 S. Huang, *Scr. Mater.*, 2019, **168**, 5–9.
30 P. Singh, A. V. Smirnov and D. D. Johnson, *Phys. Rev. B: Condens. Matter Mater. Phys.*, 2015, **91**, 1–12.
31 W. Kohn and L. J. Sham, *Phys. Rev.*, 1965, **140**, 1133–1138.
32 F. Tian, L. K. Varga, N. Chen, L. Delczeg and L. Vitos, *Phys. Rev. B: Condens. Matter Mater. Phys.*, 2013, **87**, 1–8.
33 L. Vitos, J. Kollar and H. L. Skriver, *Phys. Rev. B: Condens. Matter Mater. Phys.*, 1994, **49**, 16694–16701.
34 P. Soven, *Phys. Rev.*, 1967, **156**, 809–813.
35 B. L. Gyorffy, *Phys. Rev. B: Solid State*, 1972, **5**, 2382–2384.
36 F. Tian, L. K. Varga, J. Shen and L. Vitos, *Comput. Mater. Sci.*, 2016, **111**, 350–358.
37 N. I. A. Zoubi, M. P. J. Punkkinen, B. Johansson and L. Vitos, *Phys. Rev. B: Condens. Matter Mater. Phys.*, 2010, **81**, 1–10.
38 Y. Pan, S. Chen and Y. L. Jia, *Int. J. Hydrogen Energy*, 2020, **45**, 6207–6216.
39 L. A. Girifalco and V. G. Weizer, *Phys. Rev.*, 1959, **114**, 687–690.
40 S. Guo, C. Ng, Z. Wang and C. T. Liu, *J. Alloys Compd.*, 2014, **583**, 410–413.
41 F. X. Zhang, S. Zhao, K. Jin, H. Bei, D. Popov, C. Park, J. C. Neuefeind, W. J. Weber and Y. Zhang, *Appl. Phys. Lett.*, 2017, **110**, 011902.
42 A. J. Zaddach, C. Niu, C. C. Koch and D. L. Irving, *JOM*, 2013, **65**, 1780–1789.
43 L. Rogal, *Mater. Des.*, 2017, **119**, 406–416.

44 S. Thangaraju, T. E. Bouzy and A. Hazotte, *Adv. Eng. Mater.*, 2017, **1700095**, 1–6.
45 H. Xiao, Y. Liu, K. Wang, Z. P. Wang, T. Hu, T. W. Fan, L. Ma and P. Y. Tang, *Acta Metall. Sin. (Engl. Lett.)*, 2020, 1–10.
46 J. F. Nye, *Physical properties of crystals: their representation by tensors and matrices*, Oxford University Press, Oxford, 1985.
47 D. Iotova, N. Kioussis and S. P. Lim, *Phys. Rev. B: Condens. Matter Mater. Phys.*, 1996, **54**, 14413–14422.
48 O. L. Anderson, *J. Phys. Chem. Solids*, 1963, **24**, 909–917.
49 F. Tian, L. Delczeg, N. Chen, L. K. Varga, J. Shen and L. Vitos, *Phys. Rev. B: Condens. Matter Mater. Phys.*, 2013, **88**, 085128.
50 H. Z. Fu, D. H. Li, F. Peng, T. Gao and X. L. Cheng, *Comput. Mater. Sci.*, 2008, **44**, 774–778.
51 H. Z. Fu, W. M. Peng and T. Gao, *Mater. Chem. Phys.*, 2009, **115**, 789–794.
52 S. F. Pugh, *Philos. Mag.*, 1954, **45**, 823–843.
53 Y. Pan, *Vacuum*, 2020, **181**, 109742.
54 H. Z. Fu, X. F. Li, W. F. Liu, Y. M. Ma, T. Gao and X. H. Hong, *Intermetallics*, 2011, **19**, 1959–1967.
55 X. Q. Chen, H. Y. Niu, D. Z. Li and Y. Y. Li, *Intermetallics*, 2011, **19**, 1275–1281.
56 Y. Pan, *ACS Sustainable Chem. Eng.*, 2020, **8**, 11024–11030.
57 K. Lau and A. K. Mccurdy, *Phys. Rev. B: Condens. Matter Mater. Phys.*, 1998, **58**, 8980–8984.
58 C. Zener, *Elasticity and anelasticity of metals*, University of Chicago Press, Chicago, 1948.
59 R. P. Ingel and D. L. Iii, *J. Am. Ceram. Soc.*, 2005, **71**, 265–271.
60 M. H. Yoo, *Scr. Metall.*, 1986, **20**, 915–920.
61 A. J. E. Foreman, *Acta Metall.*, 1955, **3**, 322–330.
62 M. M. Savin, V. M. Chernov and A. M. Strokova, *Phys. Status Solidi A*, 1976, **35**, 747–754.
63 C. N. Reid, *Acta Metall.*, 1966, **14**, 13–16.